ACS APPLIED MATERIALS & INTERFACES

Research Article

www.acsami.org

Facile Synthesis of Different Morphologies of Cu_2SnS_3 for High-Performance Supercapacitors

Chao Wang,*[,†] Hanqing Tian,[†] Jing Jiang,[†] Ting Zhou,[†] Qing Zeng,[†] XinRui He,[†] Pei Huang,[†] and Yan Yao[‡]

[†]Clean Energy Materials and Engineering Center, School of Microelectronics and Solid-State Electronics, State Key Laboratory of Electronic Thin Film and Integrated Device, University of Electronic Science and Technology of China, Chengdu Sichuan, China

[‡]Department of Electrical & Computer Engineering and Materials Science and Engineering Program, University of Houston, Houston, Texas 77204, United States

Supporting Information

ABSTRACT: Cu_2SnS_3 is considered as an emerging potential candidate for electrode materials due to considerable interlayer spaces and tunnels in its crystal structures and excellent conducting ability. Ternary Cu_2SnS_3 as anode in lithium ion batteries has already been reported, but it is rarely mentioned to be applied in supercapacitors which is considered to be a complementary energy storage device for lithium ion batteries. It is an effective method to improve the electrochemical performance of materials by adjusting the morphology and microstructure of materials. In present study, ternary nanosheet-assembled Cu_2SnS_3 microspheres (M-CTS) and nanoparticles-like Cu_2SnS_3 (N-CTS) are synthesized via a facile solvothermal route. The results suggest that Cu_2SnS_3 microspheres (M-CTS) exhibit better capacitive performance compared with Cu_2SnS_3 (N-CTS) nanoparticles, which means that morphology does have a significant effect on the electrochemical reaction. M-CTS presents excellent supercapacitor performances with the high specific capacity of about 406 C g^{-1} at a current density of 1 A g^{-1} and achieves a high energy density of 85.6 W h kg^{-1} and power density of 720 W kg^{-1}. The remarkable electrochemical performance of Cu_2SnS_3 can be attributed to the large specific surface area, smaller average pore size, and improved electrical conductivity. Our research indicates that it is very suitable for large-scale production and has enormous potential in the practical application of high-performance supercapacitors.

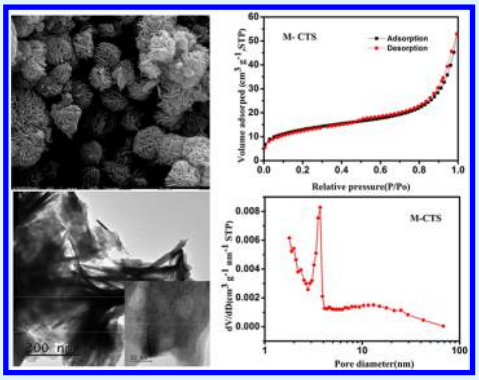

KEYWORDS: *Cu_2SnS_3, morphology, microspheres, high performance, supercapacitor*

1. INTRODUCTION

The urgent demands for high power, high density, and sustainable energy sources compel us to search for novel alternative storage devices. At the same time, faced with increasing portable devices, it is more urgent to find some storage devices which can be efficient and safe for storing energy. Therefore, the emergence of supercapacitors have changed the situation to a certain degree. Supercapacitors, also called electrochemical capacitors, are a significant type of energy storage device and widely studied because of its high power density, short charge−discharging time, and long cycle life.[1−4] In the light of their energy storage mechanism, supercapacitors could be classified into electrical double-layer capacitors (EDLCs)[5] and pseudocapacitors (PCs). A large accumulation of charge at the electrode/electrolyte interface is the main source of capacitance for electric double-layer capacitors (EDLCs). However, the capacitance of the pseudocapacitors (PCs) is mainly derived from fast and reversible faradic redox reactions occurring on the electrode surface.

In recent years, the electrode materials of supercapacitors have not been limited to carbon-based materials, transition-metal oxides, and conducting polymers. Transition-metal sulfides, which is a fascinating class among the electrode materials such as CuS, FeS_2, SnS_2, Ni_2S_3, and SnS, have also been extensively studied for its potential applications in electrochemical energy storage devices.[6−8] Zhang et al. found a simple in situ growth process that produced a three-dimensional (3D) interconnected CuS nanowall on Ni foam, exhibiting excellent performance at a current density of 15 mA cm^{-2}. The improved electrochemical performance may be dependent on the high conductivity and large specific surface area.[9] Wang et al. also found that novel three-dimensional flower-like heterostructured SnS_2/MoS_2 was prepared through a facile hydrothermal method, which showed good cycling stability even after 1000 cycles.[10] Li et al. have also found that grasslike Ni_3S_2 nanorod/nanowire arrays grown on the NF network were synthesized by precisely regulating the oxidation degree of the NF precursor, achieving a high specific capacitance of 4.52 F cm^{-2} at 1.25 mA cm^{-2} and showing superior cycling stability.[11] Chauhan et al. reported that SnS nanorods exhibit mediocre supercapacitor performance[12] with

Received: May 21, 2017
Accepted: July 24, 2017
Published: July 24, 2017

DOI: 10.1021/acsami.7b07190
ACS Appl. Mater. Interfaces 2017, 9, 26038−26044

specific capacitance value of about 70 F g^{-1}. It is proved that the specific surface is indeed a critical parameter to determine the specific capacitance of these electrode materials.[13] These researching results demonstrate that special morphological structure of the material really have remarkable advantage.[14−16] Moreover, SnS has been proven to have potentially excellent properties for application in photovoltaic devices and electrochemical capacitors. But its application in supercapacitors has been hindered by the lower specific capacitance. One of the reasons is poor electrical conductivity compared with other metal sulfides. Through adding copper into stannous sulfide (SnS), Cu_2SnS_3 with enhanced electrical conductivity has been extensively investigated for the purpose of improving the electrochemical performance. In addition, Cu_2SnS_3 (CTS), a ternary semiconductor compound, is an emerging potential candidate for electrode materials and consists of three elements, namely, copper, tin, and sulfur. These elements are abundant on earth and are nontoxic. Hence, it is very suitable for large-scale production, which will alleviate energy shortages.

Since Cu_2SnS_3 exhibits the enormous interlayer spaces and tunnels in its crystal structures,[17] and higher theoretical capacity, it is the first attempt to apply CTS to supercapacitors in this work. Therefore, in our study we have synthesized CTS samples with different morphologies through one-step solvothermal method and electrochemical performances of CTS are investigated. In contrast to stannous sulfide (SnS), CTS has performed better specific capacitance. The nanosheet-assembled Cu_2SnS_3 microspheres (M-CTS) can reach about 406 C g^{-1} at current densities of 1 A g^{-1}, which is higher than that of Cu_2SnS_3 nanoparticles (N-CTS) (about 313 C g^{-1}). Because of the unique structure of nanosheet-assembled microspheres, the specific surface area of M-CTS (44.9 m^2 g^{-1}) is almost twice than that of N-CTS (28.2 m^2 g^{-1}),which exhibits stupendous advantages, including rich accessible electroactive sites, sufficient transmission channels, and added ion transport pathways. So it is more conducive to the occurrence of electrochemical reactions and getting better electrochemical performance. When the M-CTS is charged and discharged at current densities of 2 A g^{-1} to 2000 cycles, about 136 C g^{-1} capacity still remained, indicating that CTS indeed has a huge potential application in terms of energy storage.

2. MATERIALS AND METHODS

2.1. Materials. $CuCl_2{\cdot}2H_2O$ (99%), $SnCl_2$ (99%), $SnCl_4{\cdot}5H_2O$ (99%), thioacetamide (99%), and thiourea (99%) used in this study were obtained from Aladdin (Shanghai, China). Nickel foam (diameter 11 mm) was rinsed ultrasonically with 1 mol L^{-1} HCl solution for 15 min and then washed three times with deionized water and absolute ethanol, respectively. Analytical-grade hydrochloric acid (HCl) and ethyl alcohol were received from ChengDu KeLong Glass Co. Ltd. (ChengDu, China). All chemicals were analytical grade and used without any further purification.

2.2. Characterization. Scanning electron microscopy (SEM) as well as electron energy-dispersive spectroscopy (EDS) were carried out using field emission scanning electron microscopy (FESEM, JSM-7600F). Transmission electron microscopy (TEM) images were collected on Tecnai G2 Spirit Twin(FEI) at 120 kV. Power X-ray diffraction (XRD) spectra were received using DX-2700B (haoyuan) diffractometer with Cu Kα radiation (λ = 1.5406 Å).

2.3. Synthesis of Cu_2SnS_3. In the typical procedure, the nanoparticles-like Cu_2SnS_3 (N-CTS) was synthesized in this way. Four millimoles of $CuCl_2{\cdot}2H_2O$, 2 mmol of $SnCl_2$ and 6 mmol of thiourea (TU) were dissolved in 30 mL of polyethylene glycol (PEG) and stirred for 2 h to be dispersed and dissolved completely. Then the mixture was transferred from a beaker to a Teflon-lined stainless steel autoclave and sealed. After that it was placed in the oven at 180 °C for 16 h without annealing. When the vessel was then cooled to room temperature, the sample was centrifuged and washed several times with deionized water and absolute ethanol, and then dried in a vacuum at 60 °C for 12 h for spare use.

The nanosheet-assembled Cu_2SnS_3 microspheres (M-CTS) was synthesized in an analogous manner. The difference in synthetic conditions is that 4 mmol of $CuCl_2{\cdot}2H_2O$, 2 mmol of $SnCl_4{\cdot}5H_2O$, and 6 mmol of thioacetamide were dissolved in 30 mL of solution with 50% ethanol and 50% water and the autoclave was sealed and maintained at 200 °C for 7.5 h. More significantly, the temperature, reaction time, and solvent are critical parameters in the solvothermal method. Any of the above parameters is changed, which will have a great influence on the morphology of the obtained sample.

2.4. Electrochemical Measurements. The electrochemical performances were investigated by three-electrode configuration using Pt sheet as counter electrode, mercuric oxide electrode as reference electrode, and nickel foam coating with the mixture electrode material as a working electrode. The working electrode was prepared with electrode material, acetylene black, and polyvinylidene fluoride (PVDF) in a mass ratio of 7:2:1 and then dropped 1-methyl-2-pyrrolidinone and was stirred for 2 h. Afterward, the mixed and ground slurry was sprayed onto the nickel foam current collectors and transformed into a vacuum oven at 60 °C for 12 h. All electrochemical measurements were carried out by a PARSTAT 4000 electrochemical workstation in 3 mol L^{-1} KOH aqueous solution. The loading of the active material was calculated on the basis of the mass difference before and after drying and the mass loading for each active material was about 1.5 mg.

3. THEORETICAL BASIS

Galvanostatic charge−discharge (GCD), cyclic voltammetry (CV), and electrochemical impedance spectroscopy (EIS) are usually adopted to appraise the electrochemical performances of electrode materials. The specific capacitance can be calculated as

$$C = I\frac{\Delta t}{m}\Delta V \tag{1}$$

where I is the discharge current, Δt is the discharge time in one cycle, ΔV is the charge and discharge voltage difference, and m is the mass of active electrode materials.[3,18] The energy density can be calculated as

$$E = \frac{1}{2}CV^2 \tag{2}$$

The power density can be calculated as

$$P = \frac{E}{\Delta t} \tag{3}$$

4. RESULTS AND DISCUSSION

4.1. Material Characterization. Different morphologies of Cu_2SnS_3 are obtained by different synthetic conditions. As shown in Figure 1a, the nanoparticles with a diameter of about 30 nm are stacked together and agglomeration is serious. More clear nanoparticles are arranged together in higher magnification in Figure 1c. Figure 1b clearly illustrates that each microsphere is constructed by several overlapping nanosheets and the diameter of each microsphere is about 600 nm. It further demonstrates the distinct nanosheet-assembled microspheres structure as shown in Figure 1d. To further illuminate the composition of the sample, we have performed the electron energy-dispersive spectroscopy (EDS). As shown in Figure 1e, EDS presents that the average atomic ratio of S:Cu:Sn is approximately 50.1:33.6:16.2. From Figure 1f, the results of EDS show that the average atomic ratio of S:Cu:Sn is approximately

DOI: 10.1021/acsami.7b07190
ACS Appl. Mater. Interfaces 2017, 9, 26038−26044

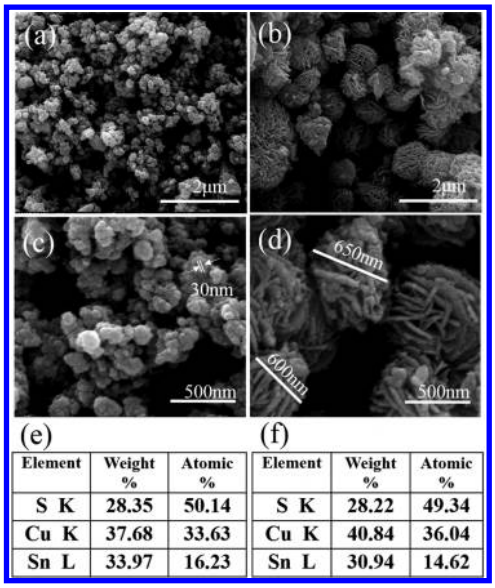

(e)

Element	Weight %	Atomic %
S K	28.35	50.14
Cu K	37.68	33.63
Sn L	33.97	16.23

(f)

Element	Weight %	Atomic %
S K	28.22	49.34
Cu K	40.84	36.04
Sn L	30.94	14.62

Figure 1. (a) and (c) Magnified SEM image of the N-CTS nanostructures; (b) and (d) magnified SEM image of the M-CTS nanostructures; (e) EDS pattern of the N-CTS nanostructures; (f) DS pattern of the M-CTS nanostructures.

49.3:36.0:14.6. Apparently, these two components are very close to stoichiometric ratio 2:1:3, which is quite consistent with the targeted elemental compositions.

Figure 2a,b presents the TEM images of N-CTS. The lattice fringe spacing is measured to be about 0.31 nm corresponding to the *d*-spacing between adjacent (111) planes of the cubic Cu_2SnS_3 structure.[19] Figure 2c,d displays the typical TEM images of M-CTS; it is noted that the internal structure of the hairball is made up of some needlelike protrusions, which shows a loose porous structure.

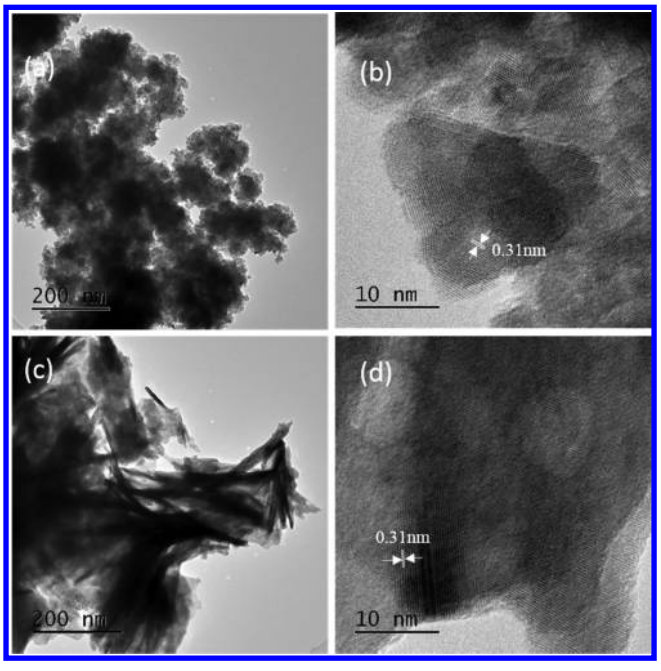

Figure 2. TEM images of Cu_2SnS_3 in different magnifications. (a) Characteristic TEM image of N-CTS at low magnification; (b) high-resolution TEM image of N-CTS; (c) characteristic TEM image of M-CTS at low magnification; (d) high-resolution TEM image of M-CTS.

Figure 3a,b illustrates the XRD patterns of N-CTS and M-CTS in this study. As shown in Figure 3a, the major XRD diffraction

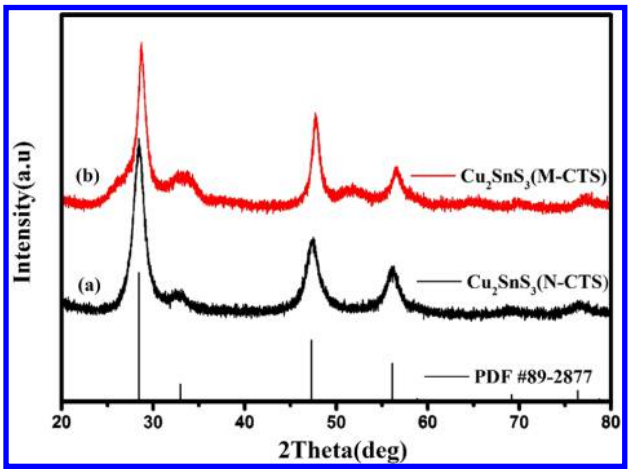

Figure 3. (a) XRD pattern of the N-CTS nanostructures; (b) XRD pattern of the M-CTS nanostructures.

peaks that appeared at $2\theta = 28.5°$, 32.8°, 47.5°, 56.4°, 68.6°, and 76.3° are corresponding to (111), (200), (220), (311), (400), and (331) of Cu_2SnS_3 (JCPDS no. 89-2877), which is in good agreement with the standard data for cubic phase of the Cu_2SnS_3. Interestingly, the peak intensity of N-CTS is higher than that of M-CTS, implying that it has better crystallinity than that of M-CTS. Furthermore, the relative intensity ratio of (111) to (220) for N-CTS is obviously higher than that of M-CTS, indicating that the processing conditions will influence the oriented growth of obtained Cu_2SnS_3 products, which is in keeping with SEM and TEM results mentioned above.

The valence and composition about the Cu_2SnS_3 are further investigated by XPS. Figure 4a illustrates the XPS spectrum of Cu 2p core level about M-CTS, implying that the observed values of the binding energies for Cu $2p_{3/2}$ and Cu $2p_{1/2}$ are about 932.0 and 951.7 eV,[20] respectively, which are consistent with the values for Cu^+. Additionally, it is also observed that a peak located at about 942 eV appears in the spectrum, indicating that divalent copper ions remain. Figure 4b shows the XPS spectrum of Cu 2p core level about N-CTS, indicating that it has equivalent values of the binding energies for Cu $2p_{3/2}$and Cu $2p_{1/2}$. The Sn 3d core splits into Sn $3d_{5/2}$ (486.4 eV) and Sn $3d_{3/2}$ (495.1 eV) peaks for M-CTS, which coincides with the reported values for Sn^{4+} as shown in Figure 4c.[20] As Figure 4d presents the Sn 3d core splits into Sn $3d_{5/2}$ (486.1 eV) and Sn $3d_{3/2}$ (494.8 eV) peaks for N-CTS. It can be concluded that the normal valence states of Cu_2SnS_3 are Cu^+, Sn^{4+}, and S^{2-}, which is also consistent with the XRD results discussed above. Two peaks appear around 338 and 295 cm^{-1}, which is similar to Chen's work as shown in Figure 4e,f.[21]

4.2. Electrochemical Performance Study. Figure 5a displays the cyclic voltammetry (CV) curves of N-CTS at various scan rates with scanning range from 0.15 to 0.65 V. It is apparent that the whole CV curves display a pair of significant redox peaks, revealing typical pseudocapacitive behavior. The only difference from the M-CTS is that when the scanning rate is 40 mV or higher than 40 mV, a couple of redox peaks become less obvious. The reason for this phenomenon needs to be further studied.

Figure 5b reveals the cyclic voltammetry (CV) curves of M-CTS at various scan rates with the same scanning range. It is

DOI: 10.1021/acsami.7b07190
ACS Appl. Mater. Interfaces 2017, 9, 26038−26044

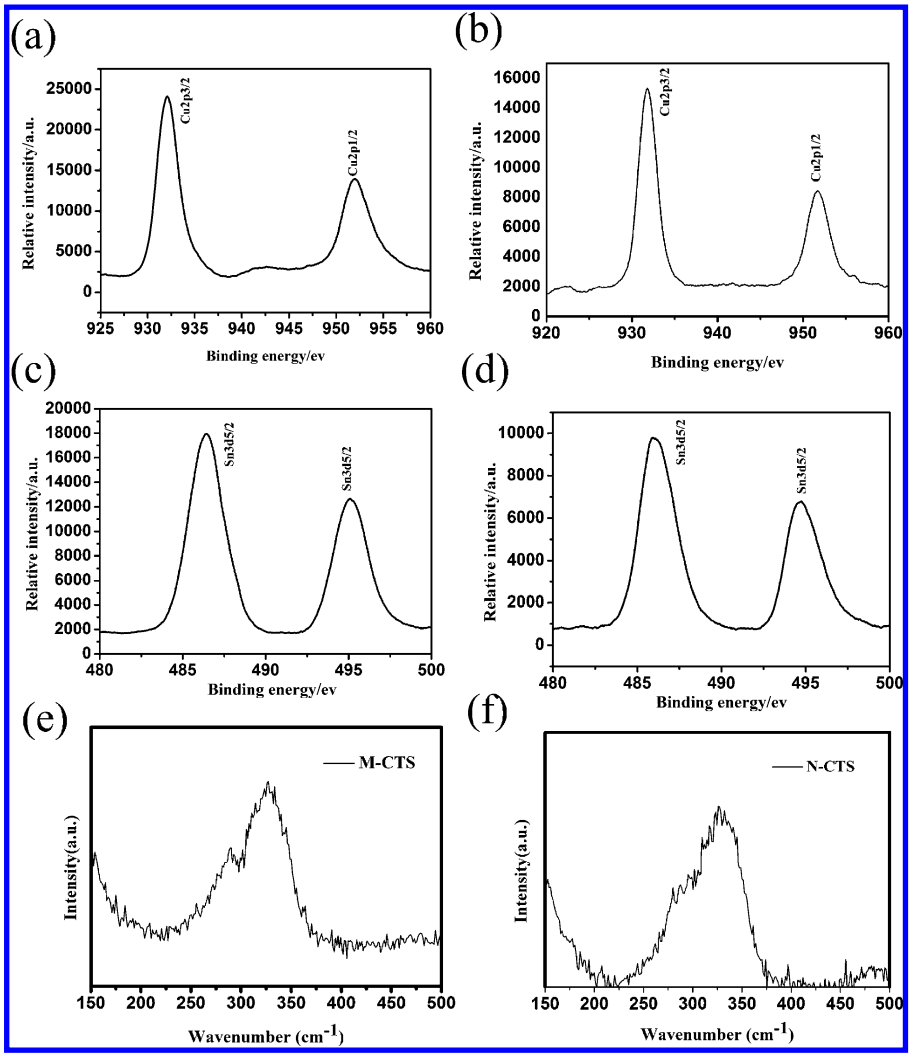

Figure 4. (a) Core level spectrum for Cu 2p of M-CTS nanostructures; (b) core level spectrum for Cu 2p of N-CTS nanostructures; (c) core level spectrum for Sn 3d of M-CTS nanostructures; (d) core level spectrum for Sn 3d of N-CTS nanostructures; (e) Raman spectrum of the obtained M-CTS samples; (f) Raman spectrum of the obtained N-CTS samples.

obvious that even if the scanning rate is 40 mV or higher than 40 mV, the couple of redox peaks is still visible, reflecting better reversibility of electrochemical reactions. The performance of GCD is also a vital parameter for assessing their potential application. Figure 5c shows the typical discharge curves of the N-CTS at galvanostatic current densities of 1, 2, 4, 8, 10, 15, and 20 A g^{-1} in the potential range of 0.13−0.53 V, respectively. The specific capacitance can be equal to 313, 288, 255, 218, 201, 157, and 126 C g^{-1} in 3 mol L^{-1} KOH aqueous solution at galvanostatic current densities of 1, 2, 4, 8, 10, 15, and 20 A g^{-1}, respectively. As the current density increases, the specific capacitance gradually decreases with increasing current density. Since the transport of various ions in the electrolyte is affected by time constraints at high current densities and just only the external active surface is used for charge storage, resulting in inadequate use of active materials.[22] Obviously, a very prominent discharge platform appears in the discharge curve, which coincides with the CV curves, indicating that it has good pseudocapacitive behavior.

Figure 5d presents the typical discharge curves of M-CTS under conditions identical to those of N-CTS, of which specific capacitance can be achieved to 406, 349, 330, 276, 253, 115, and 101 C g^{-1} at current densities of 1, 2, 4, 8, 10, 15, and 20 A g^{-1}, respectively. As the data show, M-CTS has better specific capacitance performance than N-CTS. The excellent electrochemical performances could be attributed to the ternary Cu_2SnS_3 where Cu, regarded as a kind of excellent electrical conductor, can improve the conductivity of the material and improved conductivity compared with SnS.

To further investigate the electrode process dynamics and analyze the mechanism of complex electrode reaction, electrochemical impedance spectroscopy (EIS) was the preferred method. A Nyquist plot was obtained in 3 mol L^{-1} KOH at frequency from 100 kHz to 0.01 Hz with an amplitude of 10 mV. The Nyquist curve consists of three components: the first part is the intersection point with the *X*-axis solid line, indicating the internal resistance of the electrode; the semicircle of the relative high-frequency band represents the interface charge-transfer resistance R_{ct} at the electrode−electrolyte interface; and the linear region of low frequency stands for the typical capacitor behavior.[23−26] Figure 6a,b illustrates the Nyquist plots of the N-CTS and M-CTS electrodes, which mainly contains a clear semicircle in the high-frequency region and a straight line in the low-frequency region. The series resistance (R_s) of N-CTS is about 1.43 Ω and M-CTS has achieved 1.67 Ω as illustrated in Figure 6b. The R_{ct} value for M-CTS is almost 0.37 Ω, which is still

DOI: 10.1021/acsami.7b07190
ACS Appl. Mater. Interfaces 2017, 9, 26038−26044

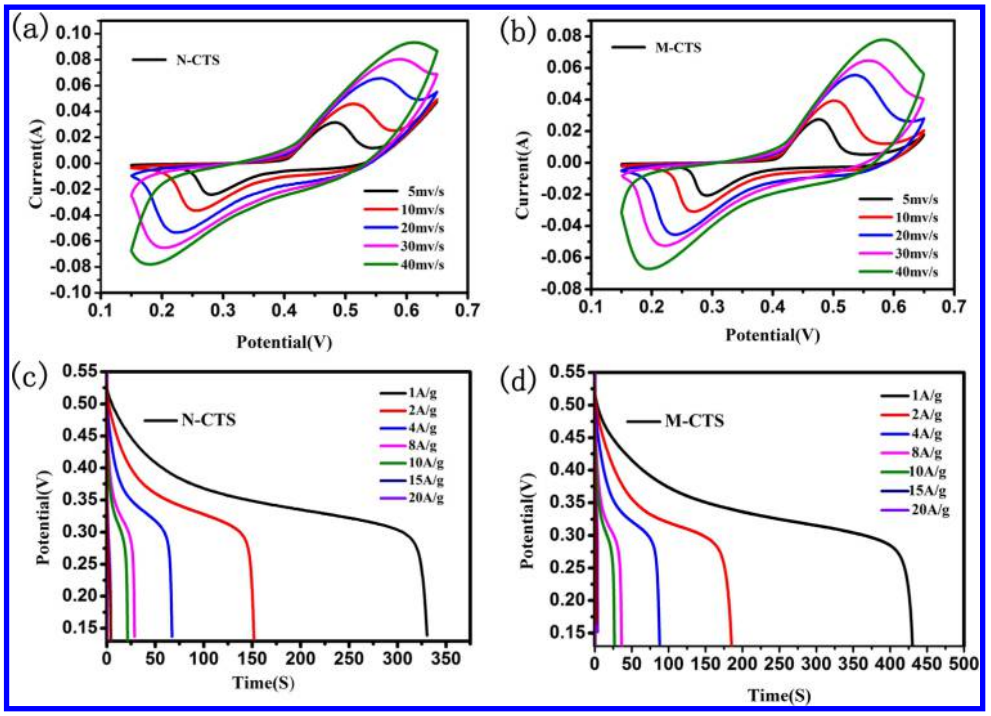

Figure 5. (a) CV curves of the N-CTS; (b) CV curves of the M-CTS; (c) GCD curves of the N-CTS at different current densities; (d) GCD curves of the M-CTS at different current densities.

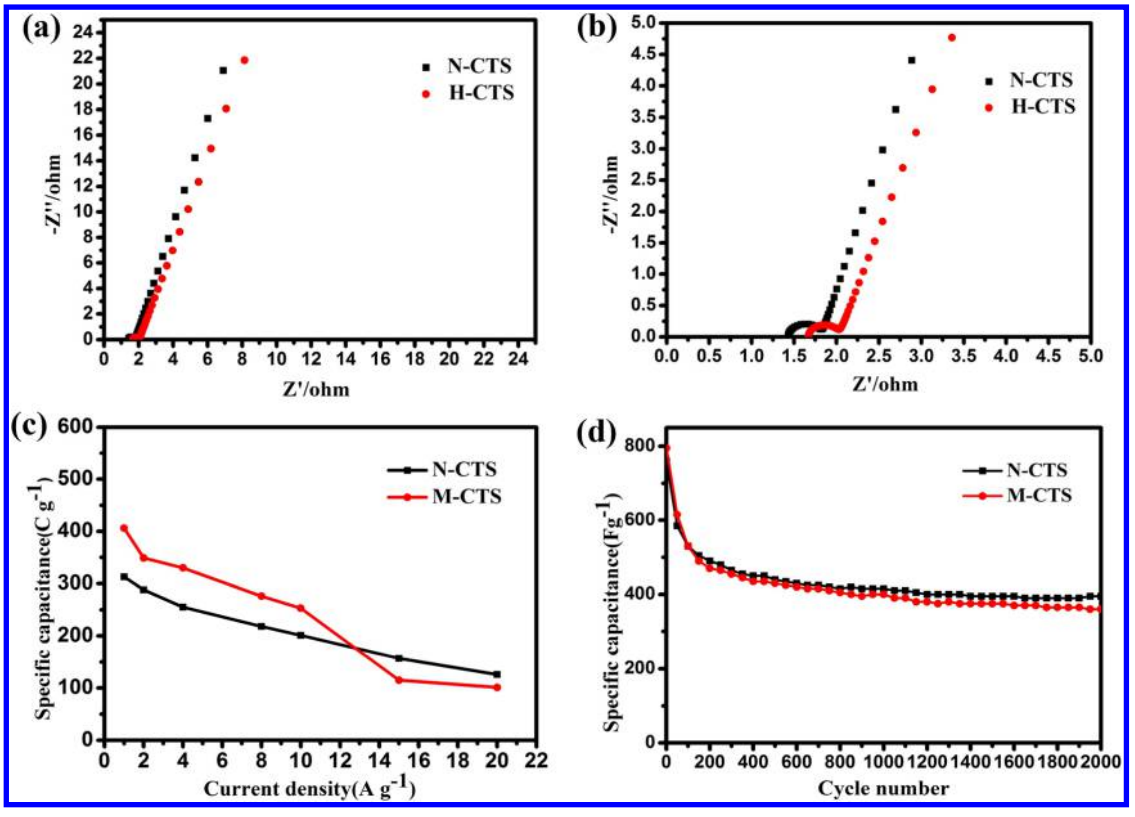

Figure 6. (a) EIS of N-CTS and M-CTS; (b) enlarged EIS of N-CTS and M-CTS; (c) comparison of the specific capacity of N-CTS to the specific capacity of M-CTS at different current densities; (d) cycling measurements at a current density of 2 A g^{-1} of N-CTS and M-CTS.

lower than the N-CTS (0.40 Ω). All in all, these two kinds of CTS electrodes exhibit a low series resistance and a nearly vertical line at the lower frequency part, suggesting that CTS is likely to be a potential alternative to supercapacitors electrode materials.

The cycling stability of the supercapacitors almost determines its service life; thus, it makes sense to study this parameter.[27] To test long-term cycling stability of electrode materials, continuous charge−discharge cycles are utilized at a constant discharge current density of 2 A g^{-1} by landian battery (CT2001A) test

DOI: 10.1021/acsami.7b07190
ACS Appl. Mater. Interfaces 2017, 9, 26038−26044

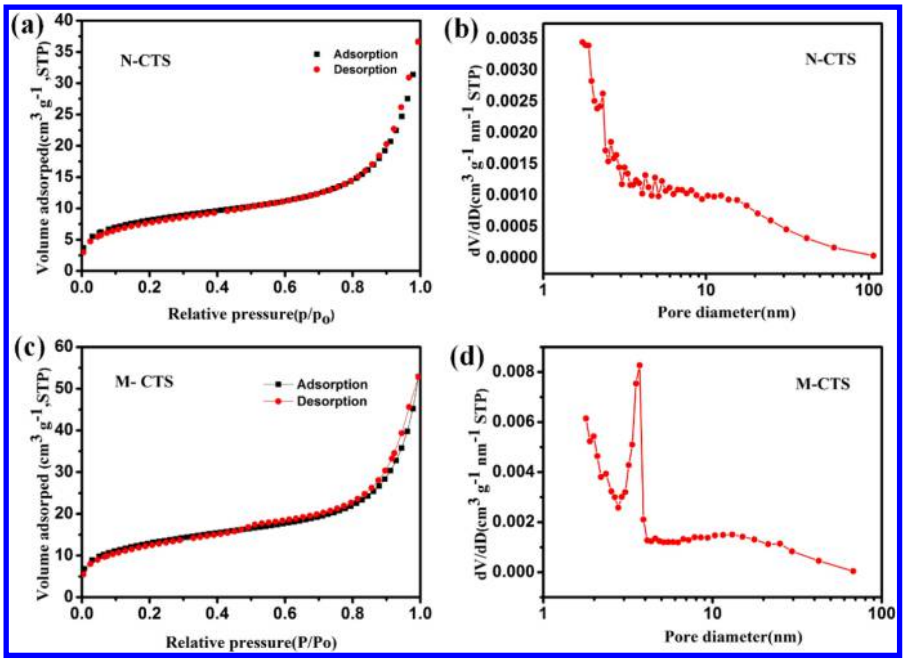

Figure 7. (a) Nitrogen adsorption and desorption isotherm graphs of the N-CTS nanostructures; (b) pore size distribution of N-CTS; (c) nitrogen adsorption and desorption isotherm graphs of the M-CTS nanostructures; (d) pore size distribution of M-CTS.

system in 3 mol L^{-1} KOH with a potential window of 0.13−0.53 V. As illustrated in Figure 6c, it demonstrates that the specific capacitance of M-CTS is about 406 C g^{-1} in the first cycle. Then the specific capacitance gradually decreases with the increasing time and approximately 60% of the initial capacity is exhausted after 2000 cycles. After 300 cycles, the specific capacitance of two kinds of CTS both become more and more stable. Although a relatively large decrease can be observed in the initial stage, this may be due to the skeleton collapse of the material and the unstable lattice structure. We have tested the SEM image of active materials after cycling to demonstrate my speculations as shown in Figure S1 in the Supporting Information. As presented in Figure 6d, the specific capacitance of the M-CTS supercapacitors is much higher than that of N-CTS supercapacitors with the same current density.

Thus, excellent pseudocapacitance and unique structure of nanosheet-assembled microspheres of M-CTS are sufficient to explain why its electrochemical performance is higher than that of N-CTS.

It has been proven that the specific surface area and pore-size distribution have an important impact on the electrochemical performance of the material.[13] To further evaluate the different electrochemical performances between N-CTS and M-CTS, the nitrogen adsorption−desorption isotherms were carried out to investigate the porous characteristics of the Cu_2SnS_3. The hysteresis loop presented in Figure 7a,c can be incorporated in type II according to the IUPAC classification. Because the size of adsorbent pore varies, it can lead to multimolecular layer adsorption based on type II.

As Figure 7a,c illustrates, the nitrogen adsorption−desorption isotherms of N-CTS and M-CTS were calculated to be 28.2 and 44.9 m^2 g^{-1}, respectively, which is consistent with the experimental results. Qu's work revealed that the BET surface area of the entire Cu_2SnS_3 nanostructures was about 22.4 m^2 g^{-1} and the average pore size of which was 13.8 nm. Obviously, our obtained samples both have a better performance in microstructure when compared with their synthetic products. The larger specific surface area of the electrode material, the more electroactive sites can be provided, and the faster transport channels of ions and charges for the electrode material.

The higher the peak indicates that the number of holes in this diameter account for the greater proportion. M-CTS has the BJH pore size distribution centered at a diameter of about 10.2 nm, which is lower than N-CTS (11.6 nm) as presented in Figure 7b,d. More electroactive sites and abundant ions transport pathway were obtained owing to the unique structure of M-CTS; meanwhile, the mesopores can shorten ions diffusion length to a certain extent, resulting in high specific capacitance performance.

5. CONCLUSIONS

In summary, two kinds of CTS with completely different morphologies were synthesized via a facile method without additional substrates. Nanosheet-assembled Cu_2SnS_3 microspheres (M-CTS) can achieve a higher specific capacitance of 406 C g^{-1} with a higher energy density of 85.6 W h kg^{-1} at a power density of 720 W kg^{-1} when compared with N-CTS (313 C g^{-1}), demonstrating that it is indeed an efficient and effective method to enhance the electrochemical performance of materials through regulating microstructures. M-CTS with larger specific surface areas and smaller average pore sizes do have a higher specific capacitance, which match the experimental results perfectly. It is also prominent that the Cu_2SnS_3 can be large-scale production due to simple and facile preparation method, which makes it closer to the practical application requirements. Our work provides a reference for the optimization of sulfide electrode materials.

■ ASSOCIATED CONTENT

Supporting Information

The Supporting Information is available free of charge on the ACS Publications website at DOI: 10.1021/acsami.7b07190.

SEM images of the N-CTS nanostructures before and after cycling; SEM images of the M-CTS nanostructures before and after cycling (PDF)

DOI: 10.1021/acsami.7b07190
ACS Appl. Mater. Interfaces 2017, 9, 26038−26044

AUTHOR INFORMATION

Corresponding Author

*E-mail: cwang@uestc.edu.cn.

ORCID

Chao Wang: 0000-0003-2167-6619

Ting Zhou: 0000-0002-5178-375X

Author Contributions

Chao Wang and Hanqing Tian contributed equally to this work.

Notes

The authors declare no competing financial interest.

ACKNOWLEDGMENTS

The work is partly funded by the Department of Science and Technology of Sichuan Province (No. 2015JY0066 and 2016JQ0022), the National Natural Science Foundation of China (No. 51672037 and 61604031), the open fund of State Key Laboratory of Advanced Welding and Joining of HIT (No. AWJ-M16-07), the Fundamental Research Funds for the Central Universities (No. ZYGX2013J115 and ZYGX2015J029), and the open fund of Laboratory of Precision Manufacturing Technology, CAEP (No. KF14008).

REFERENCES

(1) Yang, Z.; Ren, J.; Zhang, Z.; Chen, X.; Guan, G.; Qiu, L.; Zhang, Y.; Peng, H. Recent Advancement of Nanostructured Carbon for Energy Applications. *Chem. Rev.* **2015**, *115* (11), 5159−5223.

(2) Xia, H.; Hong, C.; Li, B.; Zhao, B.; Lin, Z.; Zheng, M.; Savilov, S. V.; Aldoshin, S. M. Facile Synthesis of Hematite Quantum-Dot/Functionalized Graphene-Sheet Composites as Advanced Anode Materials for Asymmetric Supercapacitors. *Adv. Funct. Mater.* **2015**, *25* (4), 627−635.

(3) Wang, Y.; Song, Y.; Xia, Y. Electrochemical Capacitors: Mechanism, Materials, Systems, Characterization and Applications. *Chem. Soc. Rev.* **2016**, *45* (21), 5925−5950.

(4) Wang, G.; Zhang, L.; Zhang, J. A Review of Electrode Materials for Electrochemical Supercapacitors. *Chem. Soc. Rev.* **2012**, *41* (2), 797−828.

(5) Borenstein, A.; Hanna, O.; Attias, R.; Luski, S.; Brousse, T.; Aurbach, D. Carbon-based Composite Materials for Supercapacitor Electrodes: a review. *J. Mater. Chem. A* **2017**, *5* (25), 12653−12672.

(6) Wang, L.; Zhang, X.; Ma, Y.; Yang, M.; Qi, Y. Supercapacitor Performances of the MoS_2/CoS_2 Nanotube Arrays in Situ Grown on Ti Plate. *J. Phys. Chem. C* **2017**, *121* (17), 9089−9095.

(7) Fu, W.; Han, W.; Zha, H.; Mei, J.; Li, Y.; Zhang, Z.; Xie, E. Nanostructured CuS Networks Composed of Interconnected Nanoparticles for Asymmetric Supercapacitors. *Phys. Chem. Chem. Phys.* **2016**, *18* (35), 24471−24476.

(8) Ma, L.; Xu, L.; Zhou, X.; Xu, X.; Zhang, L. Molybdenum-doped Few-layered SnS_2 Architectures with Enhanced Electrochemical Supercapacitive Performance. *RSC Adv.* **2015**, *5* (128), 105862−105868.

(9) Zhang, Y.; Xu, J.; Zheng, Y.; Hu, X.; Shang, Y.; Zhang, Y. Interconnected CuS Nanowalls with Rough Surfaces Grown on Nickel foam as High-performance Electrodes for Supercapacitors. *RSC Adv.* **2016**, *6* (65), 59976−59983.

(10) Wang, L.; Ma, Y.; Yang, M.; Qi, Y. One-pot Synthesis of 3D Flower-like Heterostructured SnS_2/MoS_2 for Enhanced Supercapacitor Behavior. *RSC Adv.* **2015**, *5* (108), 89069−89075.

(11) Li, T.; Zuo, Y.; Lei, X.; Li, N.; Liu, J.; Han, H. Regulating the Oxidation Degree of Nickel Foam: a Smart Strategy to Controllably Synthesize Active Ni_3S_2 Nanorod/Nanowire Arrays for High-performance Supercapacitors. *J. Mater. Chem. A* **2016**, *4* (21), 8029−8040.

(12) Chauhan, H.; Singh, M. K.; Hashmi, S. A.; Deka, S. Synthesis of Surfactant-free SnS Nanorods by a Solvothermal Route with Better Electrochemical Properties towards Supercapacitor Applications. *RSC Adv.* **2015**, *5* (22), 17228−17235.

(13) Lee, G.; Lee, C.; Yoon, C.-M.; Kim, M.; Jang, J. High-Performance Three-Dimensional Mesoporous Graphene Electrode for Supercapacitors using Lyophilization and Plasma Reduction. *ACS Appl. Mater. Interfaces* **2017**, *9* (6), 5222−5230.

(14) Wu, N.; Zhang, Y.; Guo, Y.; Liu, S.; Liu, H.; Wu, H. Flakelike $LiCoO_2$ with Exposed {010} Facets As a Stable Cathode Material for Highly Reversible Lithium Storage. *ACS Appl. Mater. Interfaces* **2016**, *8* (4), 2723−2731.

(15) Wang, Y.; Huang, S.; Lu, Y.; Cui, S.; Chen, W.; Mi, L. High-rate-capability Asymmetric Supercapacitor Device Based on Lily-like Co_3O_4 Nanostructures Assembled using Nanowires. *RSC Adv.* **2017**, *7* (7), 3752−3759.

(16) Tang, Y.; Chen, S.; Chen, T.; Guo, W.; Li, Y.; Mu, S.; Yu, S.; Zhao, Y.; Wen, F.; Gao, F. Synthesis of peanut-like Hierarchical Manganese Carbonate Microcrystals via Magnetically Driven self-assembly for High Performance Asymmetric Supercapacitors. *J. Mater. Chem. A* **2017**, *5* (8), 3923−3931.

(17) Wu, C.; Hu, Z.; Wang, C.; Sheng, H.; Yang, J.; Xie, Y. Hexagonal Cu_2SnS_3 with Metallic Character: Another category of conducting sulfides. *Appl. Phys. Lett.* **2007**, *91* (14), 143104.

(18) Liu, Q.; Lu, C.; Li, Y. Controllable Synthesis of Ultrathin Nickel Oxide Sheets on Carbon Cloth for High-performance Supercapacitors. *RSC Adv.* **2017**, *7* (37), 23143−23148.

(19) Qu, B.; Li, H.; Zhang, M.; Mei, L.; Chen, L.; Wang, Y.; Li, Q.; Wang, T. Ternary Cu_2SnS_3 Cabbage-like Nanostructures: Large-scale Synthesis and Their Application in Li-ion Batteries with Superior Reversible Capacity. *Nanoscale* **2011**, *3* (10), 4389−93.

(20) Liang, X.; Cai, Q.; Xiang, W.; Chen, Z.; Zhong, J.; Wang, Y.; Shao, M.; Li, Z. Preparation and Characterization of Flower-like Cu_2SnS_3 Nanostructures by Solvothermal Route. *J. Mater. Sci. Technol.* **2013**, *29* (3), 231−236.

(21) Chen, Q.; Ma, D. Preparation of Nanostructured Cu_2SnS_3 Photocatalysts by Solvothermal Method. *Int. J. Photoenergy* **2013**, *2013*, 593420.

(22) Ruan, Y.; Jiang, J.; Wan, H.; Ji, X.; Miao, L.; Peng, L.; Zhang, B.; Lv, L.; Liu, J. Rapid Self-assembly of Porous Square Rod-like Nickel Persulfide via a Facile Solution Method for High-performance Supercapacitors. *J. Power Sources* **2016**, *301*, 122−130.

(23) Li, Y.; Cao, L.; Qiao, L.; Zhou, M.; Yang, Y.; Xiao, P.; Zhang, Y. Ni-Co Sulfide Nanowires on Nickel Foam with Ultrahigh Capacitance for Asymmetric Supercapacitors. *J. Mater. Chem. A* **2014**, *2* (18), 6540−6548.

(24) Dall'Agnese, Y.; Taberna, P.-L.; Gogotsi, Y.; Simon, P. Two-Dimensional Vanadium Carbide (MXene) as Positive Electrode for Sodium-Ion Capacitors. *J. Phys. Chem. Lett.* **2015**, *6* (12), 2305−2309.

(25) Li, Y.; Chang, S.; Liu, X.; Huang, J.; Yin, J.; Wang, G.; Cao, D. Nanostructured CuO Directly Grown on Copper Foam and Their Supercapacitance Performance. *Electrochim. Acta* **2012**, *85*, 393−398.

(26) Zhang, Z.; Liu, X.; Qi, X.; Huang, Z.; Ren, L.; Zhong, J. Hydrothermal Synthesis of Ni_3S_2/graphene Electrode and its Application in a Supercapacitor. *RSC Adv.* **2014**, *4* (70), 37278−37283.

(27) Zhang, G.; Xiao, X.; Li, B.; Gu, P.; Xue, H.; Pang, H. Transition Metal Oxides with One-dimensional/One-dimensional-analogue Nanostructures for Advanced Supercapacitors. *J. Mater. Chem. A* **2017**, *5* (18), 8155−8186.

DOI: 10.1021/acsami.7b07190
ACS Appl. Mater. Interfaces 2017, 9, 26038−26044